Available online at www.sciencedirect.com

ScienceDirect

journal homepage: www.elsevier.com/locate/he

Polypyrrole assisted synthesis of nanosized iridium oxide for oxygen evolution reaction in acidic medium

Jian Zhang [a,b], *Shiyu Liu* [a], *Hao Wang* [a], *Qibin Xia* [b], *Xiaoxi Huang* [a,*]

[a] *Hoffmann Institute of Advanced Materials, Postdoctoral Innovation Practice Base, Shenzhen Polytechnic, 7098 Liuxian Blvd, Nanshan District, Shenzhen, 518055, PR China*

[b] *School of Chemistry and Chemical Engineering, South China University of Technology, Guangzhou, 510640, PR China*

HIGHLIGHTS

- Nanosized IrO_2 was synthesized by using polypyrrole (PPY) as soft template.
- Temperature influences the electrochemical active surface area (ECSA) of the IrO_2.
- PPY endows the as-synthesized IrO_2 with higher ECSA and better OER performance.

GRAPHICAL ABSTRACT

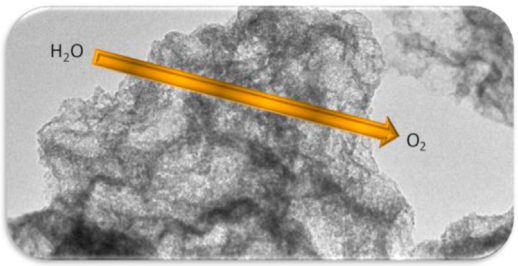

ARTICLE INFO

Article history:
Received 6 July 2020
Received in revised form
28 August 2020
Accepted 11 September 2020
Available online xxx

Keywords:
Iridium oxide
Oxygen evolution reaction
Soft template
Polypyrrole

ABSTRACT

The application of electrochemical water splitting process in acidic medium is restricted by the lack of highly efficient and stable oxygen evolution reaction (OER) electrocatalyst. In this work, we report a facile soft template method to synthesize nanosized iridium oxide for electrocatalytic OER in acidic medium. The fabrication process involves thermal treatment of iridium complex and polypyrrole in air. The compositions and structures of the resulting catalytic materials are significantly influenced by the annealing temperature. The nanostructured iridium oxide synthesized at optimal 450 °C exhibits low overpotential (291.3 ± 6 mV) to reach 10 mA/cm^2 current density towards OER, which is better than the commercial iridium oxide. Further investigation indicates that nanosized iridium oxide synthesized at 450 °C has high electrochemical active surface area to expose abundant accessible active sites, which can accelerate the OER rate. This method can also provide new guidance to prepare other metal oxide nanoparticles for various applications.

* *Corresponding author.*
E-mail address: xiaoxihuang@szpt.edu.cn (X. Huang).

https://doi.org/10.1016/j.ijhydene.2020.09.089
0360-3199/

Introduction

To meet the rapid development of worldwide economy, a large amount of fossil fuels such as coal, oil and natural gas have been consumed, resulting in serious environmental problems. The sustainable and renewable energy sources including solar, wind, tidal, etc., have attracted much attention among researchers. Electrochemical water splitting plays an important role for the efficient utilization of these intermittent clean energy sources [1–3], however, the overall water splitting process is predominantly limited by the sluggish kinetics of oxygen evolution reaction (OER), due to the complicated four electrons transfer process [4–6]. Despite considerable progress has been made to search for highly efficient catalysts for OER in alkaline electrolyte, it remains a great challenge to develop active and stable electrocatalysts which can operate in acidic solution for proton exchange membrane (PEM) electrolyzer [7–9].

So far, ruthenium- and iridium-based materials are the most active electrocatalysts in acidic medium with low OER overpotential [10–17]. However, the instability of ruthenium-based metal oxides in acidic medium limited the practical application in OER, even though they show a higher activity. In contrast, iridium-based electrocatalysts not only have reasonable activity but also the durable stability in acidic electrolyte [5,18–24]. Nevertheless, the scarcity and high cost of iridium element calls for the exploration of simple methods to improve the utilization of iridium as much as possible for OER. This can be resolved by developing iridium based electrocatalysts with improved electrochemical active surface area (ECSA) and more accessible active sites to catalyze OER. Nanostructuring is an effective strategy to improve the ECSA of electrocatalysts. One of the approaches is to use template-assisted method to endow iridium oxide with a porous structure, such as mesoporous silica [25], silica colloidal crystal [26] based hard templates, and polymer based soft templates [27–29]. Other template-free methods like ammonia-assisted strategy can also improve the surface area and porosity of iridium oxide [30]. In comparison with hard templates, using soft templates is appealing as they can be removed more readily to produce porosity. Compared with other soft templates based on oxygen containing polymers, nitrogen containing polypyrrole (PPY) may provide more coordination sites to bind with metal precursors, and therefore lead to more uniform dispersion of metal precursors in the polymer matrix. To the best of our knowledge, PPY has not been used as soft template to synthesize iridium based porous materials.

Here we report a soft template method to synthesize nanosized iridium oxide with improved OER performance via annealing iridium complex embedded PPY nanocomposites. The influence of annealing temperature for the fabricated electrocatalysts towards the electrochemical OER activity is investigated. Notably, to achieve 10 mA/cm^2 current density, the catalyst prepared at 450 °C only requires 291.3 ± 6 mV overpotential, which is 42 mV lower than the overpotential of a commercial IrO_2 catalyst. The improved OER performance is ascribed to its high ECSA along with more exposed active sites.

Experimental section

Materials

Ammonium hexachloroiridate (IV) and iridium oxide were purchased from Macklin Biochemical Co., Ltd. Ammonium persulfate, sulfuric acid, and pyrrole were all obtained from Shanghai Aladdin Biochemical Co., Ltd. Nafion 117 solution were obtained from Sigma Aldrich. All the reagents were of analytical grade and used as received without further purification. Deionized water supplied by Aquaplore 2S system and used throughout the experiments.

Preparation of electrocatalyst

2 g of ammonium persulfate and 0.1 g of ammonium hexachloroiridate (IV) was completely dissolved in 6 mL and 18 mL deionized water, forming solution A and B, respectively. Solution B was rapidly poured into solution A. Then 0.608 mL of pyrrole was quickly added to the above mixed solution under vigorously stirring. The mixed solution was stirred between 0 and 5 °C for 4 h in an ice bath. Subsequently, the solvent was removed via lyophilization to yield iridium complex embedded PPY nanocomposites. 0.5 g of the obtained nanocomposites were then placed in a corundum crucible boat and heated from 50 to 450 °C at a rate of 5 °C min^{-1} and maintained at the target temperature for 1 h in muffle furnace. After cooling down to room temperature, the obtained solid was washed with deionized water by centrifugation (10,000 rpm for 4 min in each time) to remove the soluble impurities. Finally, the resulting material was dried overnight at 65 °C and denoted as PPY-Ir-450. Other samples prepared under identical conditions except for different annealing temperatures at 350 °C, 400 °C and 500 °C were named as PPY-Ir-350, PPY-Ir-400 and PPY-Ir-500, respectively.

Characterization

Powder X-ray diffraction patterns (XRD) of the catalysts were recorded with an Empyrean PANalytical in the 2θ range 10°–80° at a step scanning rate of 0.5° min^{-1} using a Cu Kα1 radiation (λ = 1.5406 Å). Transmission electron microscope (TEM) images were obtained by using FEI Talos 200S transmission electron microscope with an accelerating voltage of 200 kV. The surface elemental compositions of the samples were confirmed by an X-ray photoelectron spectroscopy (XPS, K-Alpha+, Thermo Fisher Scientific) equipped with a monochromatic Al Ka X-ray source. The specific surface area of the samples were measured using N_2 adsorption/desorption isotherms at 77 K (Micromeritics 3Flex analyzer). The Fourier Transform Infrared (FTIR) was performed on Frontier FTIR spectrometer with ATR from 4000 to 650 cm^{-1} (PerkinElmer).

Electrochemical measurement

The electrocatalytic oxygen evolution activities of the catalysts were evaluated with a CHI 660E (CH Instruments Ins.) electrochemical workstation in 0.5 M H_2SO_4 electrolyte. A standard one compartment three-electrode system composed

Please cite this article as: Zhang J et al., Polypyrrole assisted synthesis of nanosized iridium oxide for oxygen evolution reaction in acidic medium, International Journal of Hydrogen Energy, https://doi.org/10.1016/j.ijhydene.2020.09.089

of a saturated calomel electrode (SCE) as reference electrode, graphitic carbon rod as counter electrode and a glassy carbon electrode (GCE) loaded with catalyst film as working electrode was used for the electrochemical measurement. To prepare the working electrode, 1 mg catalyst powder was uniformly dispersed in 200 μL deionized water via ultrasonication for 20 min to form the catalyst ink, then 2 μL of this suspension was applied on the surface of polished GCE (diameter: 3 mm) to form a catalyst film with a loading of 142 μg cm^{-2}. After allowing the film to dry under ambient condition, 2 μL of Nafion solution (0.5 wt %) was deposited on the top of it and also dried at room temperature.

The calibration of reference electrode was conducted based on a previously reported method [11]. In this work, all potentials (vs. SCE) were converted into the reversible hydrogen electrode (RHE) scale following the equation $E_{vs.\ RHE} = E_{vs.\ SCE} + 0.255$ V. Cyclic voltammetry (CV), linear scan voltammetry (LSV), Tafel and chronopotentiometry measurements were carried out using potentiostat to evaluate the electrochemical OER activity. LSV curves were collected at a low scan rate (5 mV/s) to minimize the influence of capacitive current, and the capacitive current background was subtracted from the recorded LSV curve. Meanwhile, the LSV was compensated by 85% *iR* - correction. The electrochemical impedance spectra were collected at a non-faradaic potential of 1.1 V from 10^5 Hz to 10^{-2} Hz, the potential amplitude was 5 mV. And high frequency range was fitted based on Randle circuit to get the single point resistance for *iR* compensation. In order to calculate electrochemical active surface area (ECSA), CV curves at potential window range from 0.9 to 1.1 V (*vs.* SCE) were recorded at various sweep rates of 5, 10, 20, 40, 60 and 80 mV s^{-1}. The electrochemical double layer capacitance (C_{dl}) was calculated by plotting the current density difference $\Delta J = (J_{anodic} - J_{cathodic})/2$ at 1.0 V (*vs.* SCE) against the scan rate, and C_{dl} equaled the slope of the linear fitted line. Specific capacitance of 0.035 mF/cm^2 was used to calculate ECSA [19].

Faradaic Efficiency measurement

To measure Faradaic Efficiency (FE) during OER, a gas-tight two-compartment H cell, separated by a Proton Exchange Membrane (N-117, Dupont), was used. Each compartment of the cell was filled with 80 mL of 0.5 M H_2SO_4. Before and during the electrochemical reaction the electrolyte solutions in both of compartments were purged continuously with high purity Ar at a constant rate of 45 sccm, which was controlled by a digital mass flow controller (Cole-Parmer). An SCE, Pt foil and a titanium foil (use hot glue to control 1 cm^2 exposed area) loaded with catalyst film were used as reference electrode, counter electrode and working electrode, respectively. The working electrode was papered by drop casting a catalyst ink containing 5 mg catalyst powder, 100 μL ethanol and 40 μL Nafiton solution (5%). The produced oxygen gas was directly vented into a gas chromatography instrument (Agilent Technologies 7890B) and detected by thermal conductivity detector (TCD). FE of oxygen gas was calculated based on the following equation [31]:

$$FE = nFV\upsilon P/(RTi)$$

where n = 4, corresponding to the number of electrons required to form O_2, V (vol%) is the volume concentration of O_2 in the gas phase, υ (m^3/s) is the gas flow rate controlled by digital mass flow controller, i (A) is the steady-state cell current, other parameters are listed here: $P = 1.01 \times 10^5$ Pa, T = 298.15 K, F = 96,485 C/mol and R = 8.314 $Jmol^{-1}$ K^{-1}.

Results and discussion

The iridium based electrocatalysts are synthesized through a two-step protocol as illustrated in Fig. 1. Iridium complex/PPY is firstly prepared via the oxidative polymerization of pyrrole in the presence of $(NH_4)_2IrCl_6$, followed by thermal annealing of the nanocomposites in air at different temperatures to allow the decomposition of PPY and inorganic salts (see more details in Electronic Supplementary Information). The obtained materials are denoted as PPY-Ir-T, where "T" represents the annealing temperature. As shown in Fig. S1, the XPS survey spectra of iridium complex/PPY reveals the presence of C, O, N, S, Ir and Cl elements. The deconvolution of high resolution N 1s XPS spectra indicates the existence of pyrrolic and ammonium nitrogen species, corresponding to the nitrogen in PPY and inorganic ammonium salts, respectively. The FTIR measurement of Iridium complex/PPY reveals a characteristic peak at ca. 3430 cm^{-1} (Fig. S2), corresponding to the N–H stretching vibrations [32,33]. Energy-dispersive X-ray spectroscopy (EDS) is further employed to probe the composition of samples annealed at different temperatures and the results are shown in Table S1. The atomic ratios of N/Ir and S/Ir were plotted in Fig. S3. When the annealing temperature is 350 °C, PPY-Ir-350 still contains substantial amount of nitrogen and sulfur, indicating that the temperature is too low and there are some organic residuals in the sample. On the contrary, the N/Ir and S/Ir ratios decrease at elevated temperatures as shown in Fig. S3, suggesting that majority of PPY and sulfate salts have been depleted when the temperature is higher than 400 °C.

To get more insights about PPY-Ir-T materials, X-ray diffraction (XRD) spectroscopy is used to study their crystal structures and the results are displayed in Fig. 2. The commercial IrO_2 is used as received for comparison purpose. It is observed that all major diffraction peaks of commercial IrO_2 can be indexed to the standard PDF card (03-065-2822) of rutile IrO_2, along with a small fraction of metallic iridium. In contrast, the characteristic peaks of iridium oxide are absent for PPY-Ir-350. Only a weak and broad peak between 20° and 30° is detected for the catalyst at 350 °C, which is attributed to the amorphous carbon produced from the decomposition of PPY, and it's in good agreement with the higher N/Ir, S/Ir ratios evidenced in Fig. S3. When the annealing temperature is increased to 400 °C, the PPY-Ir-400 nanomaterial still predominantly shows amorphous feature at this relatively low temperature. With increasing annealing temperature to 450 °C, the XRD pattern shows the broad diffraction peaks corresponding to rutile IrO_2, indicating that it has lower crystallinity and smaller grain size in comparison with commercial IrO_2. At even higher temperature (500 °C), PPY-Ir-500 displays relatively weak and broad diffraction peaks

Please cite this article as: Zhang J et al., Polypyrrole assisted synthesis of nanosized iridium oxide for oxygen evolution reaction in acidic medium, International Journal of Hydrogen Energy, https://doi.org/10.1016/j.ijhydene.2020.09.089

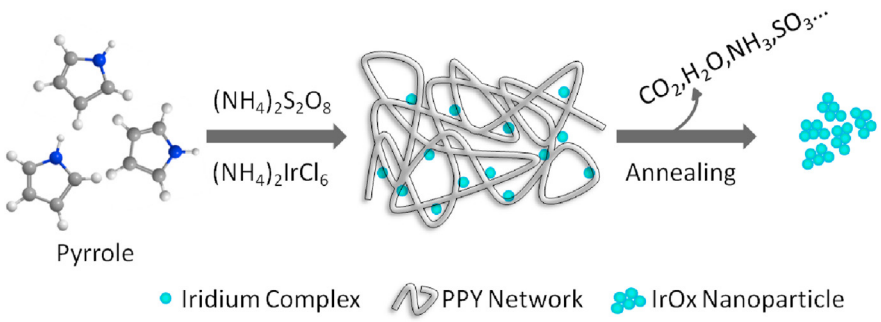

Fig. 1 – Schematic illustration of the synthetic procedures for PPY-Ir-T nanomaterials.

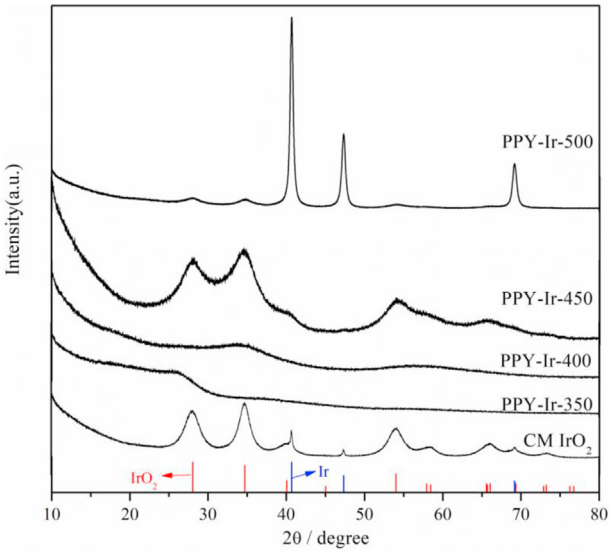

Fig. 2 – Comparison of XRD patterns for PPY-Ir-T catalysts and commercial IrO_2.

corresponding to iridium oxide at 2θ values of about 28.1° (110), 34.5° (101) and 54.7° (211), respectively. On the basis of Scherrer formula and the diffraction peak for (101), the IrO_2 crystallite domain sizes in PPY-Ir-450 and PPY-Ir-500 are calculated to be 2.2 nm and 3.9 nm, these values are smaller than CM-IrO_2, whose average grain size equals 5.1 nm. Besides, additional three sharp peaks associated with metallic iridium are observed for PPY-Ir-500, suggesting that PPY can reduce Ir (IV) species at this temperature. The metallic iridium crystallite diameter, calculated from Scherrer formula based on diffraction peak at 40.7°, is found to be 19.9 nm.

The morphologies of PPY-Ir-T catalysts are evaluated by transmission electron microscope (TEM). It seems that the microstructure of catalysts changed with annealing temperature significantly. PPY-Ir-350 reveals granule shape aggregate and the particle is amorphous based on TEM images (Fig. 3a and b), this is because it contains large amount of nitrogen/sulfur containing organic residuals. At 400 °C, a porous structure constructed by wrinkled nanosheet is observed for PPY-Ir-400 (Fig. 3c), whereas the lattice fringes are still missing in HRTEM images (Fig. 3d). When 450 °C is selected for annealing process, PPY-Ir-450 keeps the porous structure (Fig. 3e) and the HRTEM image confirms that this catalyst is composed of small nanoparticles less than 5 nm (Fig. 3f). Some orientation of lattice fringes can be observed, implying the formation of randomly oriented iridium oxide nanocrystals. A d-spacing of 0.32 nm (inset of Fig. 3f) is obtained for PPY-Ir-450, corresponding to lattice spacing of IrO_2 (110) [34]. The porous structure and small particle size of PPY-Ir-450 is beneficial to improve its catalytic performance and will be discussed in detail later. The TEM images of PPY-Ir-500 (Fig. 3g and h) show polydispersed nanoparticles with larger diameters. In addition, lattice fringes with two different d-spacing can be observed separately in the inset of Fig. 3h for PPY-Ir-500, one is 0.32 nm for iridium oxide (110) plane and the other one is 0.22 nm indexed to metallic iridium (111) plane [35], in line with XRD results. Besides the above catalysts, the TEM image (Fig. S4) of the CM-IrO_2 displays the aggregates of relatively larger particles, consistent with the XRD observation.

The surface chemical structures of PPY-Ir-T catalysts are studied by X-ray photoelectron spectroscopy (XPS) (Fig. 4). Fig. 4a reveals two distinct peaks at binding energy of 63.2 and 66.2 eV for PPY-Ir-350, which can be assigned to the moiety of iridium binding with chloride [36,37], indicating that the temperature is too low to produce IrO_2. When the temperature is increased to 400 °C, two shoulder peaks become visible at 62.0 and 65.0 eV (Fig. 4b), attributable to Ir $4f_{7/2}$ and Ir $4f_{7/2}$ of Ir(IV) oxide species. In terms of PPY-Ir-450, the primary peaks shift to 62.3 and 65.3 eV (Fig. 4c), indicating that iridium complex has been converted into IrO_2 and the oxidation state of Ir is +4 [38]. When further increasing the annealing temperature, apart from the peaks associated with Ir(IV), two additional peaks appear at lower binding energy of 61.2 and 64.2 eV (Fig. 4d), due to the formation of metallic iridium in PPY-Ir-500 [37], in line with above observations in XRD and TEM.

The surface areas and pore size distributions were measured by N_2 gas adsorption/desorption technique. The isotherms in Fig. 5a indicate that PPY-Ir-350 and PPY-Ir-400 has the lowest surface area, and the isotherms of other three catalysts show typical type IV adsorption with H3 hysteresis loop, suggesting the existence of random pore structures [39]. The pore size distribution curves in Fig. 5bc confirm that PPY-Ir-450, PPY-Ir-500 and CM-IrO_2 catalysts contain a broad range of mesopores and macropores. The BET surface areas and pore volumes of the above catalysts are summarized in Table S2. It's clear that catalysts synthesized at lower temperature have smaller surface area and pore volume, suggesting that the nanosize Ir-based particles formed at

Please cite this article as: Zhang J et al., Polypyrrole assisted synthesis of nanosized iridium oxide for oxygen evolution reaction in acidic medium, International Journal of Hydrogen Energy, https://doi.org/10.1016/j.ijhydene.2020.09.089

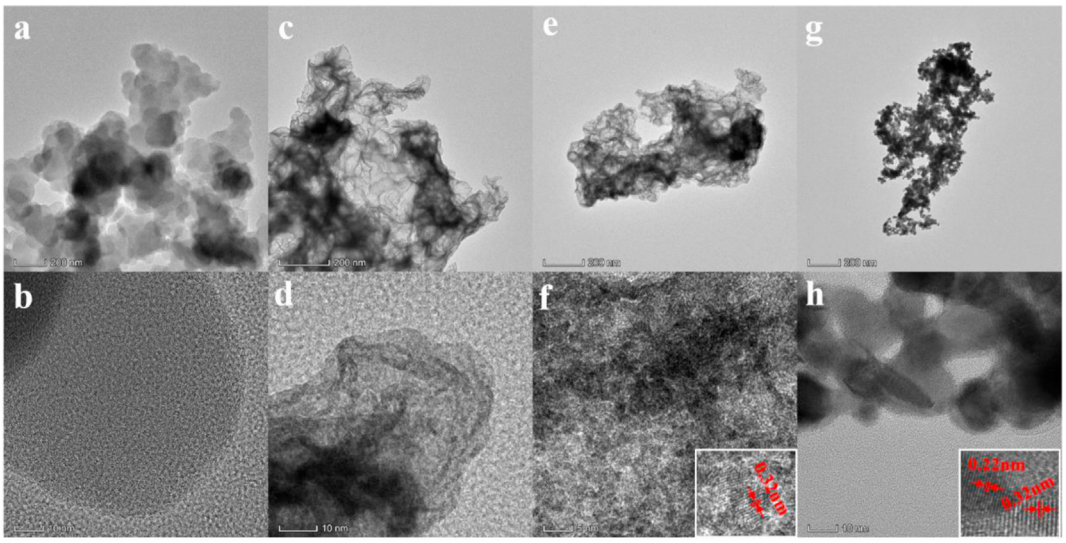

Fig. 3 – TEM and HRTRM images of catalysts synthesized at different temperatures: (a–b) 350 °C; (c–d) 400 °C; (e–f) 450 °C; and (g–h) 500 °C.

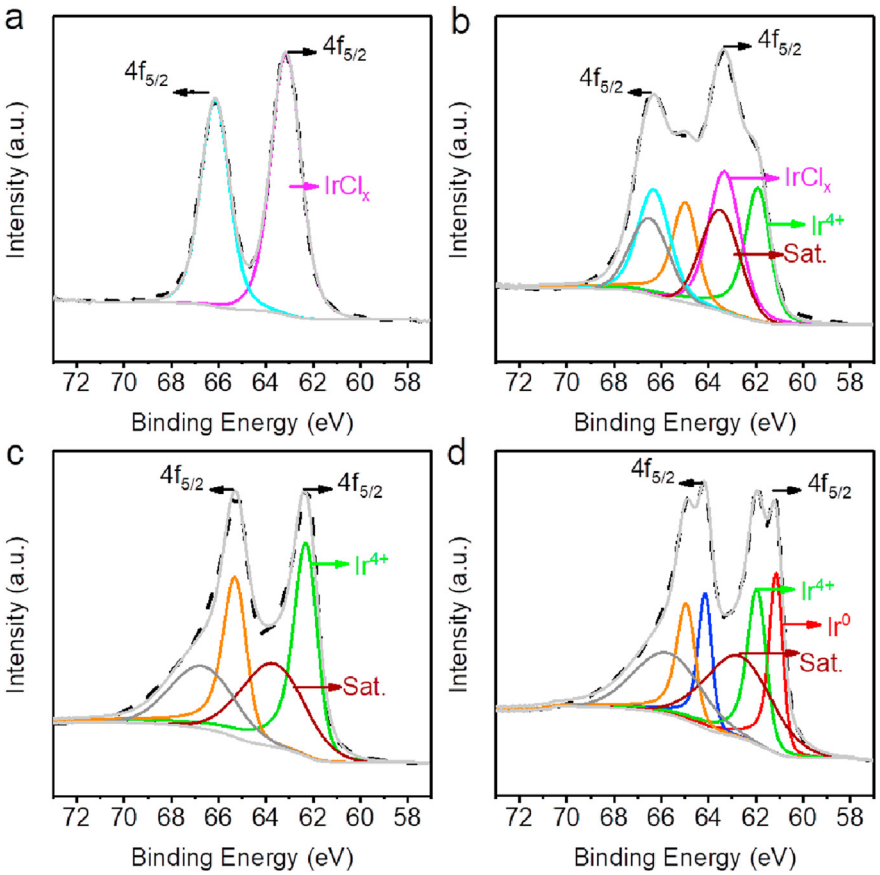

Fig. 4 – Deconvolution of high resolution Ir 4f XPS spectra for PPY-Ir-T nanocatalysts synthesized at (a) 350, (b) 400, (c) 450 and (d) 500 °C.

higher temperature can contribute more to the improved surface area.

The electrocatalytic OER performance of PPY-Ir-T is evaluated by linear scan voltammetry (LSV) in 0.5 M H_2SO_4 electrolyte. As displayed in polarization curves normalized by geometric area of glassy carbon electrode (Fig. 6a), PPY-Ir-350 shows negligible current density, which is attributed to the low surface area/pore volume, and absence of the active IrO_2 phase in the catalyst. Among all the samples, PPY-Ir-450 offers the highest OER rate as evidenced by the rapid

Please cite this article as: Zhang J et al., Polypyrrole assisted synthesis of nanosized iridium oxide for oxygen evolution reaction in acidic medium, International Journal of Hydrogen Energy, https://doi.org/10.1016/j.ijhydene.2020.09.089

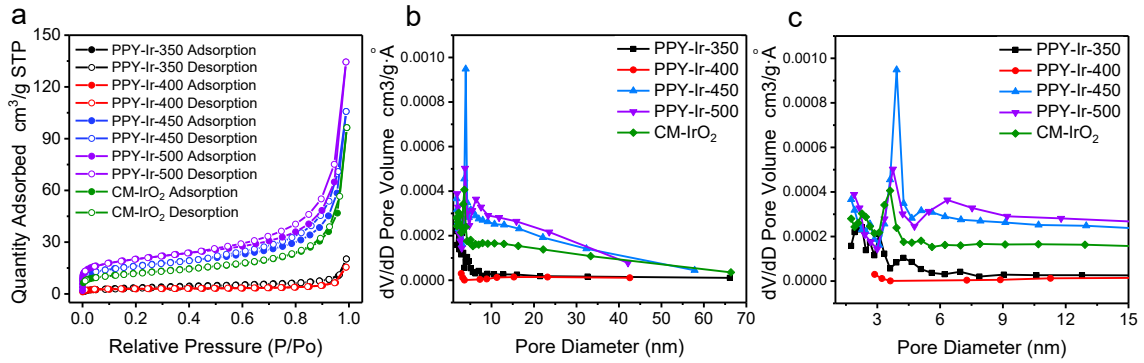

Fig. 5 – (a) The N_2 adsorption/desorption isotherms and (b) BJH pore size distribution curves for PPY-Ir-350, PPY-Ir-400, PPY-Ir-450, PPY-Ir-500 and CM-IrO_2. (c) The enlarged pore size distribution curves in the range below 15 nm.

increasing of anodic current density. The overpotential required to reach 10 mA cm^{-2} for PPY-Ir-450 is 291.3 ± 6 mV, which is 43.6 mV lower than PPY-Ir-400 and 54.3 mV lower than PPY-Ir-500 (Fig. 6b). In addition, the commercial IrO_2 need a higher overpotential (333.3 ± 9 mV mV) to reach the same current density, and the mass activity of PPY-Ir-450 is higher than CM-IrO_2 (Fig. 6c), indicating that 450 °C is the optimal temperature to synthesize highly active iridium based OER electrocatalyst using PPY as soft template. The Tafel slopes for PPY-Ir-400, PPY-Ir-450, PPY-Ir-500 and commercial IrO_2 are 64.3 mV dec^{-1}, 49.5 mV dec^{-1}, 78.2 mV dec^{-1} and 76.3 mV dec^{-1} (Fig. 6d), respectively. The lowest Tafel slope for PPY-Ir-450 implies that it has faster reaction kinetics towards OER among these catalysts. To further understand the reason for the catalytic activity gap between PPY-Ir-450 and other catalysts, ECSA is measured via double-layer capacitance. The annealing temperature can strongly impact the ECSA of as-synthesized catalysts. The CV curves of catalysts annealed at different temperatures along with commercial IrO_2 under a series of scan rates (5, 10, 20, 40, 60 and 80 mV s^{-1}) in a non-faradaic potential window are obtained to calculate ECSA (Fig. S5 and Fig. 7a).

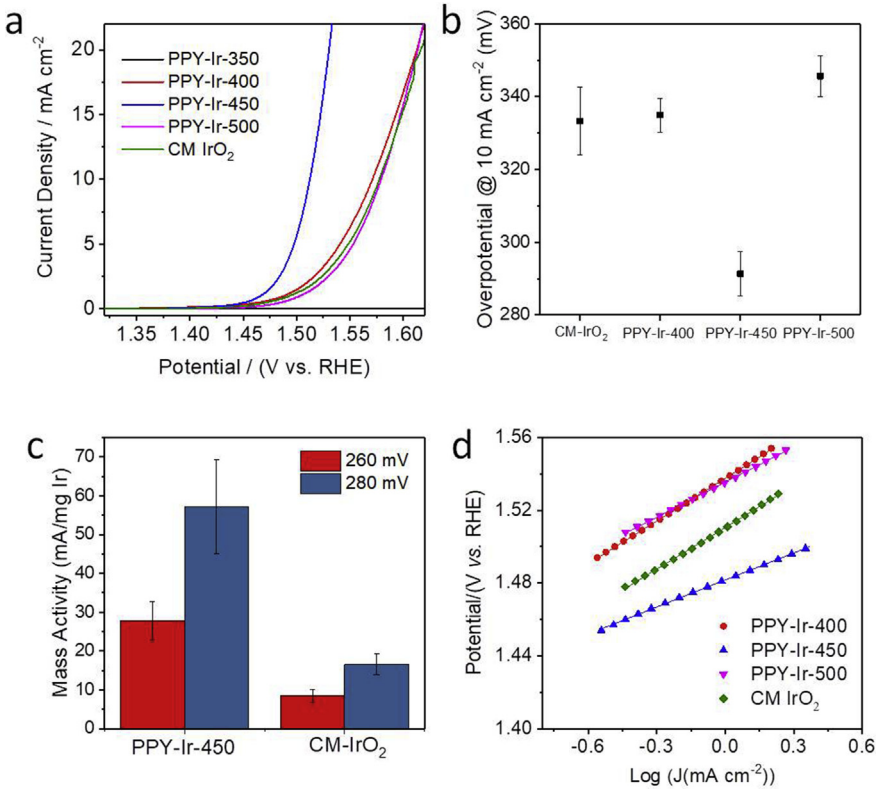

Fig. 6 – (a) Polarization curves for PPY-Ir-T catalysts and commercial IrO_2 using 0.5 M H_2SO_4 electrolyte at a scan rate of 5 mV s^{-1} after 85% *iR* correction. (b) Comparison of the overpotential required to drive 10 mA cm^{-2} current density, the results were averaged from 4 repeated experiments. (c) Comparison of the mass activity for PPY-Ir-450 and CM-IrO_2 at 260 mV and 280 mV overpotential. (d) Tafel plots of PPY-Ir-T catalysts and commercial IrO_2.

Please cite this article as: Zhang J et al., Polypyrrole assisted synthesis of nanosized iridium oxide for oxygen evolution reaction in acidic medium, International Journal of Hydrogen Energy, https://doi.org/10.1016/j.ijhydene.2020.09.089

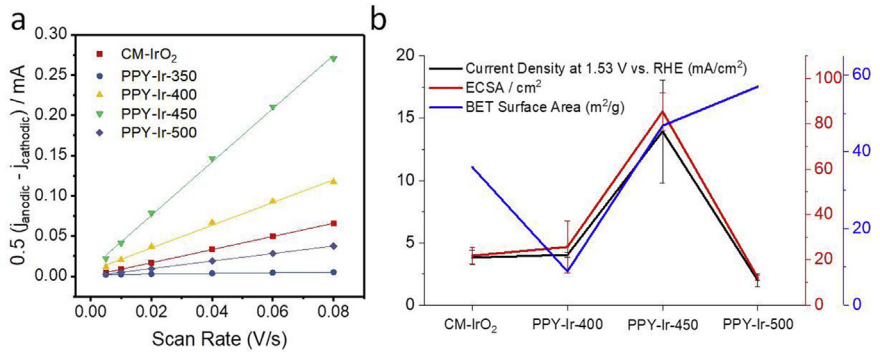

Fig. 7 – (a) Linear fitting curves of capacitive current *vs.* scan rate for the calculation of double-layer capacitance (C_{dl}). (b) Comparison of the geometric current density at 1.53 V vs. RHE (black curve), the ECSA of the catalysts (red curves) and BET surface areas (blue curve). (For interpretation of the references to color in this figure legend, the reader is referred to the Web version of this article.)

It seems that PPY-Ir-450 has the largest C_{dl}, corresponding to the highest ECSA among all the catalysts. The improved ECSA plays essential role to provide more accessible active sites on the surface for catalyzing the OER reaction, and thus leading to outstanding electrocatalytic performance. The comparison of ECSA values and the current densities normalized by geometric area for these catalysts indicate that higher ECSA lead to higher catalytic activity (Fig. 7b). However, higher BET surface area doesn't guarantee higher catalytic activity. For example, PPY-Ir-500 has the highest BET surface area, but the catalytic activity is low. We believe that this is because PPY-Ir-500 contains some less active metallic iridium nanoparticles with larger diameters. These results substantiate that the improved ECSA is the most important factor that lead to higher catalytic activity for PPY-Ir-450, which possess abundant low coordinated sites on the surface of nanosized particles. The broad CV curves (Fig. S6) from 0 to 1.4 V vs. RHE of PPY-Ir-T show a minor anodic peak ca. 1.0 V due to the transformation of Ir (III) to Ir (IV). Based on the overpotential required to reach 10 mA/cm^2 OER current density, PPY-Ir-450 is at least comparable to some previously reported iridium based catalysts (Table S3).

The above observed catalytic trends are in accordance with the combination of XRD, TEM, and XPS analysis results. 450 °C is the optimal temperature to burn off the soft template, simultaneously produce nanosized IrO_x particles with plenty of accessible surface active sites to boost the OER rate. Thermal annealing at higher temperature will lead to further growth of nanoparticles and form metallic iridium species, resulting in lower ECSA. When the annealing temperature is lower than 450 °C, catalytic active nanosized IrO_x phase does not form, and the iridium species may still bind with halide atoms, as a result, the overall OER rate is small. The presence of PPY during the annealing process can help to prevent the growth and aggregation of nanoparticles. To further prove the importance of PPY for the promoted electrocatalytic activity, several catalysts were synthesized by using less amount of PPY, namely, 20%, 10%, 2% and 1% of PPY, compared with PPY-Ir-450 under otherwise same conditions. The LSV curves (Fig. 8a) indicate that the catalytic performance becomes worse for the catalysts synthesized with less PPY, demonstrating that the presence of PPY during the synthesis is vital to achieve better OER catalytic activity. Moreover, there's a positive correlation between the ECSA and OER catalytic activity of these catalysts (Fig. 8b). When the PPY content decreases, the ECSA of the catalysts also

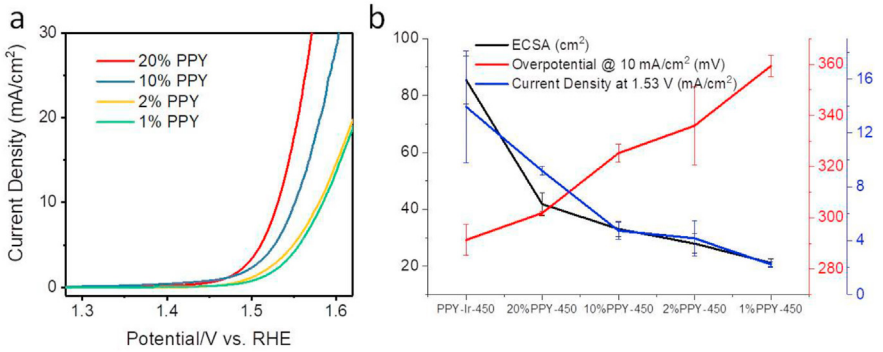

Fig. 8 – (a) Comparison of the OER performance in 0.5 M H_2SO_4 solution at the scan rate of 5 mV s^{-1} with 85% iR – correction for catalysts synthesized with different amounts of PPY templates at 450 °C. (b) Plots of ECSA (black curve), overpotential to reach 10 mA/cm^2 (red curve) and current density at 1.53 V vs. RHE for PPY-Ir-450 and catalysts prepared with less PPY templates. (For interpretation of the references to color in this figure legend, the reader is referred to the Web version of this article.)

Please cite this article as: Zhang J et al., Polypyrrole assisted synthesis of nanosized iridium oxide for oxygen evolution reaction in acidic medium, International Journal of Hydrogen Energy, https://doi.org/10.1016/j.ijhydene.2020.09.089

reduces, and it's associated with the increasing overpotential to reach 10 mA/cm^2 catalytic current. This is because the decomposition of PPY can generate gaseous products during annealing process to prevent the agglomeration of nanoparticles, and endow the resulting material with high ECSA, therefore higher catalytic activity.

The stability of OER electrocatalyst is also a critical criterion for practical applications. The long-term stability of PPY-Ir-450 and commercial iridium oxide is compared by chronopotentiometric curves in 0.5 M H_2SO_4 at a constant current density of 5 mA/cm^2 (Fig. S7). It's observed that PPY-Ir-450 can catalyze OER for at least 12 h, however, the catalytic activity of CM-IrO_2 significantly deactivates after 6 h. This result implies that PPY-Ir-450 has increased stability compared with CM-IrO_2. In addition, the oxygen FE of PPY-Ir-450 was determined in a gas-tight H-type electrochemical cell, and the FE was found to be 99%.

Conclusion

To conclude, we demonstrate for the first time that PPY can be used as soft template to synthesize active and stable OER catalyst in acidic condition. Through the method of adjusting annealing temperature, the structure of IrO_x can be tuned to improve the catalytic performance. The optimal temperature to remove the template is 450 °C. At relatively low temperature, the obtained catalysts have low surface area and iridium still bind with chloride strongly, whereas further heating triggers the fusion and growth of nanoparticles, resulting in low ECSA. The electrochemical tests confirm the importance of high ECSA for the application in OER electrocatalysis, because the total number of accessible active sites to catalyze OER scale directly with the ECSA of the catalyst. The synthetic method in this work can provide new guidance to synthesize other metal oxide nanomaterials with high ECSA for the application in electrocatalysis.

Declaration of competing interest

The authors declare that they have no known competing financial interests or personal relationships that could have appeared to influence the work reported in this paper.

Acknowledgements

We thank Shenzhen Polytechnic for support of this work. This study is supported by Post-doctoral Foundation Project of Shenzhen Polytechnic 6020330007K.

Appendix A. Supplementary data

Supplementary data to this article can be found online at https://doi.org/10.1016/j.ijhydene.2020.09.089.

REFERENCES

[1] Zou X, Zhang Y. Noble metal-free hydrogen evolution catalysts for water splitting. Chem Soc Rev 2015;44:5148–80.
[2] Seh ZW, Kibsgaard J, Dickens CF, Chorkendorff I, Norskov JK, Jaramillo TF. Combining theory and experiment in electrocatalysis: insights into materials design. Science 2017;355:eaad4998.
[3] Siwal SS, Yang W, Zhang Q. Recent progress of precious-metal-free electrocatalysts for efficient water oxidation in acidic media. J Energy Chemistry 2020;51:113–33.
[4] Grimaud A, Diaz-Morales O, Han B, Hong WT, Lee YL, Giordano L, et al. Activating lattice oxygen redox reactions in metal oxides to catalyse oxygen evolution. Nat Chem 2017;9:457–65.
[5] Carmo M, Fritz DL, Mergel J, Stolten D. A comprehensive review on PEM water electrolysis. Int J Hydrogen Energy 2013;38:4901–34.
[6] Suen NT, Hung SF, Quan Q, Zhang N, Xu YJ, Chen HM. Electrocatalysis for the oxygen evolution reaction: recent development and future perspectives. Chem Soc Rev 2017;46:337–65.
[7] Feng J, Lv F, Zhang W, Li P, Wang K, Yang C, et al. Iridium-based multimetallic porous hollow nanocrystals for efficient overall-water-splitting catalysis. Adv Mater 2017;29:1703798.
[8] Reier T, Nong HN, Teschner D, Schlögl R, Strasser P. Electrocatalytic oxygen evolution reaction in acidic environments - reaction mechanisms and catalysts. Adv Energy Mater 2017;7:1601275.
[9] Gu X-K, Camayang JCA, Samira S, Nikolla E. Oxygen evolution electrocatalysis using mixed metal oxides under acidic conditions: challenges and opportunities. J Catal 2020;388:130–40.
[10] Seitz LC, Dickens CF, Nishio K, Hikita Y, Montoya J, Doyle A, et al. A highly active and stable IrO_x/$SrIrO_3$ catalyst for the oxygen evolution reaction. Science 2016;353:1011–4.
[11] Lebedev D, Povia M, Waltar K, Abdala PM, Castelli IE, Fabbri E, et al. Highly active and stable iridium pyrochlores for oxygen evolution reaction. Chem Mater 2017;29:5182–91.
[12] Kim J, Shih PC, Tsao KC, Pan YT, Yin X, Sun CJ, et al. High-performance pyrochlore-type yttrium ruthenate electrocatalyst for oxygen evolution reaction in acidic media. J Am Chem Soc 2017;139:12076–83.
[13] Moreno-Hernandez IA, MacFarland CA, Read CG, Papadantonakis KM, Brunschwig BS, Lewis NS. Crystalline nickel manganese antimonate as a stable water-oxidation catalyst in aqueous 1.0 M H_2SO_4. Energy Environ Sci 2017;10:2103–8.
[14] Lee Y, Suntivich J, May KJ, Perry EE, Shao-Horn Y. Synthesis and activities of rutile IrO_2 and RuO_2 nanoparticles for oxygen evolution in acid and alkaline solutions. J Phys Chem Lett 2012;3:399–404.
[15] Yoo H, Oh K, Lee YR, Row KH, Lee G, Choi J. Simultaneous co-doping of RuO_2 and IrO_2 into anodic TiO_2 nanotubes: a binary catalyst for electrochemical water splitting. Int J Hydrogen Energy 2017;42:6657–64.
[16] Puthiyapura VK, Mamlouk M, Pasupathi S, Pollet BG, Scott K. Physical and electrochemical evaluation of ATO supported IrO_2 catalyst for proton exchange membrane water electrolyser. J Power Sources 2014;269:451–60.
[17] Siracusano S, Van Dijk N, Payne-Johnson E, Baglio V, Aricò AS. Nanosized IrOx and IrRuOx electrocatalysts for the O_2 evolution reaction in PEM water electrolysers. Appl Catal B Environ 2015;164:488–95.
[18] Spori C, Kwan JTH, Bonakdarpour A, Wilkinson DP, Strasser P. The stability challenges of oxygen evolving

catalysts: towards a common fundamental understanding and mitigation of catalyst degradation. Angew Chem Int Ed 2017;56:5994–6021.
[19] Yang L, Yu G, Ai X, Yan W, Duan H, Chen W, et al. Efficient oxygen evolution electrocatalysis in acid by a perovskite with face-sharing IrO_6 octahedral dimers. Nat Commun 2018;9:5236.
[20] Liang X, Shi L, Liu Y, Chen H, Si R, Yan W, et al. Activating inert, nonprecious perovskites with iridium dopants for efficient oxygen evolution reaction under acidic conditions. Angew Chem Int Ed 2019;58:7631–5.
[21] Yang L, Chen H, Shi L, Li X, Chu X, Chen W, et al. Enhanced iridium mass activity of 6H-phase, Ir-based perovskite with nonprecious incorporation for acidic oxygen evolution electrocatalysis. ACS Appl Mater Interfaces 2019;11:42006–13.
[22] Wu G, Zheng X, Cui P, Jiang H, Wang X, Qu Y, et al. A general synthesis approach for amorphous noble metal nanosheets. Nat Commun 2019;10:4855.
[23] Gao R, Zhang Q, Chen H, Chu X, Li G-D, Zou X. Efficient acidic oxygen evolution reaction electrocatalyzed by iridium-based 12L-perovskites comprising trinuclear face-shared IrO_6 octahedral strings. J Energy Chem 2020;47:291–8.
[24] Lu Z-X, Shi Y, Yan C-F, Guo C-Q, Wang Z-D. Investigation on IrO_2 supported on hydrogenated TiO_2 nanotube array as OER electro-catalyst for water electrolysis. Int J Hydrogen Energy 2017;42:3572–8.
[25] Li G, Yu H, Song W, Dou M, Li Y, Shao Z, et al. A hard-template method for the preparation of IrO_2, and its performance in a solid-polymer-electrolyte water electrolyzer. ChemSusChem 2012;5:858–61.
[26] Hu W, Wang Y, Hu X, Zhou Y, Chen S. Three-dimensional ordered macroporous IrO_2 as electrocatalyst for oxygen evolution reaction in acidic medium. J Mater Chem 2012;22:6010.
[27] Chandra D, Sato T, Takeuchi R, Li D, Togashi T, Kurihara M, et al. Polymer surfactant-assisted tunable nanostructures of amorphous IrO_x thin films for efficient electrocatalytic water oxidation. Catal Today 2017;290:51–8.
[28] Ortel E, Reier T, Strasser P, Kraehnert R. Mesoporous IrO_2 films templated by PEO-PB-PEO block-copolymers: self-assembly, crystallization behavior, and electrocatalytic performance. Chem Mater 2011;23:3201–9.
[29] Chandra D, Abe N, Takama D, Saito K, Yui T, Yagi M. Open pore architecture of an ordered mesoporous IrO_2 thin film for highly efficient electrocatalytic water oxidation. ChemSusChem 2015;8:795–9.
[30] Li G, Li S, Xiao M, Ge J, Liu C, Xing W. Nanoporous IrO_2 catalyst with enhanced activity and durability for water oxidation owing to its micro/mesoporous structure. Nanoscale 2017;9:9291–8.
[31] Zhu W, Michalsky R, Metin O, Lv H, Guo S, Wright CJ, et al. Monodisperse Au nanoparticles for selective electrocatalytic reduction of CO_2 to CO. J Am Chem Soc 2013;135:16833–6.
[32] Pech-Rodríguez WJ, González-Quijano D, Vargas-Gutiérrez G, Rodríguez-Varela FJ. Electrophoretic deposition of polypyrrole/Vulcan XC-72 corrosion protection coatings on SS-304 bipolar plates by asymmetric alternating current for PEM fuel cells. Int J Hydrogen Energy 2014;39:16740–9.
[33] Yavuz A, Ozdemir N, Zengin H. Polypyrrole-coated tape electrode for flexible supercapacitor applications. Int J Hydrogen Energy 2020;45:18876–87.
[34] Chen J, Cui P, Zhao G, Rui K, Lao M, Chen Y, et al. Low-coordinate iridium oxide confined on graphitic carbon nitride for highly efficient oxygen evolution. Angew Chem Int Ed 2019;58:12540–4.
[35] Zhang J, Wang G, Liao Z, Zhang P, Wang F, Zhuang X, et al. Iridium nanoparticles anchored on 3D graphite foam as a bifunctional electrocatalyst for excellent overall water splitting in acidic solution. Nanomater Energy 2017;40:27–33.
[36] El-Issa BD, Katrib A, Ghodsian R, Salsa BA, Addassi SH. A comparative study of the bonding in different halides of iridium. Int J Quant Chem 1988;33:195–216.
[37] Escard J, Pontvianne B, Contour JP. Etude par spectroscopie de photoelectrons des interactions metal—support dans des catalyseurs a l'iridium depose sur des oxydes metalliques. J Electron Spectrosc Relat Phenom 1975;6:17–26.
[38] Pfeifer V, Jones TE, Velasco Vélez JJ, Massué C, Arrigo R, Teschner D, et al. The electronic structure of iridium and its oxides. Surf Interface Anal 2016;48:261–73.
[39] Yao N, Cao S, Yeung KL. Mesoporous TiO_2–SiO_2 aerogels with hierarchal pore structures. Microporous Mesoporous Mater 2009;117:570–9.

Please cite this article as: Zhang J et al., Polypyrrole assisted synthesis of nanosized iridium oxide for oxygen evolution reaction in acidic medium, International Journal of Hydrogen Energy, https://doi.org/10.1016/j.ijhydene.2020.09.089